

Squeezing Flow of an Electrically Conducting Casson Fluid by Hermite Wavelet Technique

PREETHAM M. P.¹, KUMBINARASIAH S.¹, RAGHUNATHA K. R.²

¹Department of Mathematics,
Bangalore University,
Bengaluru,
INDIA

²Department of Mathematics,
Davangere University,
Davangere,
INDIA

Abstract: - The squeezing flow of an electrically conducting Casson fluid has been occupied in the report. The governing magneto-hydrodynamic equations transformed into highly nonlinear ordinary differential equations. The Hermite wavelet technique (HWM) resolves the consequential equation numerically. The outcomes of the Hermite wavelet and numerical approaches are remarkably identical. Through this, it is confirmed that we can solve such problems with the help of the Hermite wavelet method. Flow properties involving material parameters are additionally mentioned and defined in the element with the graphical resource. It is determined that magnetic subject is used as a managed occurrence in several flows because it normalizes the drift property. In addition, squeeze range theatre is a crucial responsibility in these sorts of issues, and an increase in squeeze variety will increase the velocity outline.

Key-Words: - Normal differential equations, Squeezing flow, Casson fluid, Hermite wavelet method, Casson fluid, Numerical method.

Received: December 19, 2022. Revised: October 26, 2023. Accepted: November 21, 2023. Published: December 22, 2023.

1 Introduction

During the end of the 20th century, the lavish and philosophical theory of wavelets was formed due to the efforts of mathematicians, physicists, and engineers. The idea of wavelets is constantly sophisticated to attempt various problems arising in different branches of sciences and engineering. Wavelet theory is one of the current up-and-coming facts in applicable mathematics. It has applications in subsequent fields, such as mathematical modeling, image processing, signal analyses, computer science, and applied sciences. The primary goal of this research is to provide a forum for multidisciplinary conversation among scientists working on diverse projects related to wavelets, fluid mechanics, and their applications. The wavelet techniques to solve nonlinear equations in fluid problems are among the recently created methodologies for the numerical solution of an equation that has received much attention, [1], [2], [3], [4], [5].

Many mechanical system paintings are beneath the principle of poignant pistons wherein plates show off the squeezing motion that is normal to their surfaces. Hydraulic lifters, engines, electric vehicles, and also have this clutching glide in a number of their components. Because sensible consequence squeezing goes with the flow between two horizontal parallel plates, its biological packages are also of identical significance. Flow interior nasogastric tubes and syringes are likewise compressing flows, [6].

Initial work on squeezing flows can be named to Stefan, who provided the fundamental method of these flows underneath the lubrication hypothesis [7]. Following him, many researchers have acknowledged that they are more at ease with squeezed flows and have achieved much technical study to understand those flows. Several contributions are noted in imminent strains [8], [9]. After that, exceptional scientists made numerous attempts to apprehend squeezing flows with an improved technique. Earlier research on squeezing flows has been based on the Reynolds equation,

whose lack of a few suitcases has been proven, [10]. Due to efforts of, [11], [12], greater supple and helpful well-known similarity transforms are availing a position. These transforms convert the Navier–Stokes equation into a highly nonlinear 4th-order normalized ordinary differential equation.

Undertaking non-Newtonian electrically fluid flow is an especially significant occurrence. In most realistic situations, we must cope with the glide of electrically conducting fluid, revealing exclusive behaviors that affect magnetic forces. In those instances, the MHD characteristic of the glide likewise had to be well thought-out. The Homotopy solution for 2D MHD squeezing float between horizontal parallel plates has been decided with the aid of, [13]. Mass and heat transfer for squeezing drift between parallel plates using the HAM is investigated, [14]. Mainly of sensible fashions, the fluids worried aren't effortless Newtonian. Highly complex rheological homes of non-Newtonian fluids cannot be studied through an available version. Different arithmetical models have been used to study diverse kinds of non-Newtonian fluids. One of the important models is the Casson fluid version. The main well-matched system to reproduce blood-like fluid flow can be studied in, [15]. It is obvious from the creative writing review that the squeezing drift of a Casson fluid among the plates shifting ordinary to their possess floor is but to be investigated. Due to the intrinsic highly nonlinearity of the governing equations, the fluid glide actual results are extremely unusual. Still, significant oversimplification assumptions had been obligatory where they may be obtainable. Those exaggeratedly obligatory suppositions may not be second-hand for greater sensible flows. Nevertheless, numerous analytical methods have been urbanized to address this obstacle that have typically been used in recent times. The variation of parameters technique (HWM) is the currently developed numerical strategy to remedy exclusive problems. Several motivating fluid flow problems are studied with the help of different wavelet methods, [16], [17], [18], [19], [20].

As per the present literature review, the above model is not considered by any mathematicians with the wavelet method. This motivates us to explain such equations via HWT. HWM is second-hand in the current work for the solution of model highly nonlinear equations. The calculated outputs are compared with the results in the literature through graphs and tables.

2 Problem Formulation

The squeezing flow of an electrically conducting Casson fluid is explained and given in, [6]

$$\left(1 + \frac{1}{\gamma}\right) F^{iv} - S(\eta F''' + 3F'' + F'F'' - FF''') - M_1^2 F'' = 0 \tag{1}$$

with suitable boundary conditions

$$F''(0) = 0, F(0) = 0, F'(1) = 0, F(1) = 1 \tag{2}$$

The relevant parameters of equations (1) and (2)

Parameter	Notation
Velocity function	F
Casson fluid parameter	γ
Squeeze number	S
Magnetic number	M_1

2.1 Process of Hermite Wavelet Matrix

The Hermite wavelet is an incessant polynomial basis wavelet, and its approximations are discussed in, [21].

2.1.1 Preparation of Operational Matrix by Integration

$$\begin{aligned} \varphi_{1,0}(x) &= \frac{2}{\sqrt{\pi}} \\ \varphi_{1,1}(x) &= \frac{1}{\sqrt{\pi}}(8x - 4) \\ \varphi_{1,2}(x) &= \frac{1}{\sqrt{\pi}}(32x^2 - 32x + 4) \\ \varphi_{1,3}(x) &= \frac{1}{\sqrt{\pi}}(128x^3 - 192x^2 + 48x + 8) \\ \varphi_{1,4}(x) &= \frac{1}{\sqrt{\pi}}(512x^4 - 1024x^3 + 384x^2 + 128x - 40) \\ \varphi_{1,5}(x) &= \frac{1}{\sqrt{\pi}}(2048x^5 - 5120x^4 + 2560x^3 + 1280x^2 - 800x + 16) \\ \varphi_{1,6}(x) &= \frac{1}{\sqrt{\pi}}(8192x^6 - 24576x^5 + 15360x^4 + 10240x^3 - 9600x^2 + 384x + 368) \\ \varphi_{1,7}(x) &= \frac{1}{\sqrt{\pi}}(32768x^7 - 114688x^6 + 86016x^5 + 71680x^4 - 89600x^3 + 5376x^2 + 10304x - 928) \\ \varphi_{1,8}(x) &= \frac{1}{\sqrt{\pi}}(131072x^8 - 524288x^7 + 458752x^6 + 458752x^5 - 716800x^4 + 57344x^3 + 164864x^2 - 29696x - 3296) \end{aligned}$$

$$\phi_{1,9}(x) = \frac{1}{\sqrt{\pi}}(524288x^9 - 2359296x^8 + 2359296x^7 + 2752512x^6 - 5160960x^5 + 516096x^4 + 1978368x^3 - 534528x^2 - 118656x + 21440)$$

$$\phi_{1,10}(x) = \frac{1}{\sqrt{\pi}}(2097152x^{10} - 10485760x^9 + 11796480x^8 + 15728640x^7 - 34406400x^6 + 4128768x^5 + 19783680x^4 - 7127040x^3 - 2373120x^2 + 857600x + 16448)$$

$$\phi_{1,11}(x) = \frac{1}{\sqrt{\pi}}(8388608x^{11} - 46137344x^{10} + 57671680x^9 + 86507520x^8 - 216268800x^7 + 30277632x^6 + 174096384x^5 - 78397440x^4 - 34805760x^3 + 18867200x^2 + 723712x - 461696)$$

$$\phi_{1,12}(x) = \frac{1}{\sqrt{\pi}}(33554432x^{12} - 201326592x^{11} + 276824064x^{10} + 461373440x^9 - 1297612800x^8 + 207618048x^7 + 1392771072x^6 - 752615424x^5 - 417669120x^4 + 301875200x^3 + 17369088x^2 - 22161408x + 561536)$$

Where,

$$\phi_9(x) = [\phi_{1,0}(x), \phi_{1,1}(x), \phi_{1,2}(x), \phi_{1,3}(x), \phi_{1,4}(x), \phi_{1,5}(x), \phi_{1,6}(x), \phi_{1,7}(x), \phi_{1,8}(x)]^T$$

Integrate the above first nine basis about x limit from 0 to x , then express as a linear combination of Hermite wavelet basis as:

$$\int_0^x \phi_{1,0}(x) dx = \left[\frac{1}{2} \quad \frac{1}{4} \quad 0 \right] \phi_9(x)$$

$$\int_0^x \phi_{1,1}(x) dx = \left[\frac{-1}{4} \quad 0 \quad \frac{1}{8} \quad 0 \quad 0 \quad 0 \quad 0 \quad 0 \quad 0 \right] \phi_9(x)$$

$$\int_0^x \phi_{1,2}(x) dx = \left[\frac{-1}{3} \quad 0 \quad 0 \quad \frac{1}{12} \quad 0 \quad 0 \quad 0 \quad 0 \quad 0 \right] \phi_9(x)$$

$$\int_0^x \phi_{1,3}(x) dx = \left[\frac{5}{4} \quad 0 \quad 0 \quad 0 \quad \frac{1}{16} \quad 0 \quad 0 \quad 0 \quad 0 \right] \phi_9(x)$$

$$\int_0^x \phi_{1,4}(x) dx = \left[\frac{-2}{5} \quad 0 \quad 0 \quad 0 \quad 0 \quad \frac{1}{20} \quad 0 \quad 0 \quad 0 \right] \phi_9(x)$$

$$\int_0^x \phi_{1,5}(x) dx = \left[\frac{-23}{3} \quad 0 \quad 0 \quad 0 \quad 0 \quad 0 \quad \frac{1}{24} \quad 0 \quad 0 \right] \phi_9(x)$$

$$\int_0^x \phi_{1,6}(x) dx = \left[\frac{116}{7} \quad 0 \quad 0 \quad 0 \quad 0 \quad 0 \quad 0 \quad \frac{1}{28} \quad 0 \right] \phi_9(x)$$

$$\int_0^x \phi_{1,7}(x) dx = \left[\frac{103}{2} \quad 0 \quad \frac{1}{32} \right] \phi_9(x)$$

$$\int_0^x \phi_{1,8}(x) dx = \left[\frac{-2680}{9} \quad 0 \right] \phi_9(x) + \frac{1}{36} \phi_{1,9}(x)$$

Hence,

$$\int_0^x \phi(x) dx = H_{9 \times 9} \phi_9(x) + \bar{\phi}_9(x)$$

where,

$$H_{9 \times 9} = \begin{bmatrix} \frac{1}{2} & \frac{1}{4} & 0 & 0 & 0 & 0 & 0 & 0 & 0 \\ \frac{-1}{4} & 0 & \frac{1}{8} & 0 & 0 & 0 & 0 & 0 & 0 \\ \frac{-1}{3} & 0 & 0 & \frac{1}{12} & 0 & 0 & 0 & 0 & 0 \\ \frac{5}{4} & 0 & 0 & 0 & \frac{1}{16} & 0 & 0 & 0 & 0 \\ \frac{-2}{5} & 0 & 0 & 0 & 0 & \frac{1}{20} & 0 & 0 & 0 \\ \frac{-23}{3} & 0 & 0 & 0 & 0 & 0 & \frac{1}{24} & 0 & 0 \\ \frac{116}{7} & 0 & 0 & 0 & 0 & 0 & 0 & \frac{1}{28} & 0 \\ \frac{103}{2} & 0 & 0 & 0 & 0 & 0 & 0 & 0 & \frac{1}{32} \\ \frac{-2680}{9} & 0 & 0 & 0 & 0 & 0 & 0 & 0 & 0 \end{bmatrix}, \bar{\phi}_9(x) = \begin{bmatrix} 0 \\ 0 \\ 0 \\ 0 \\ 0 \\ 0 \\ 0 \\ 0 \\ 0 \\ \frac{1}{36} \phi_{1,9}(x) \end{bmatrix}$$

Next, the double integration of the above nine bases is given below.

$$\int_0^x \int_0^x \phi_{1,0}(x) dx dx = \left[\frac{3}{16} \quad \frac{1}{8} \quad \frac{1}{32} \quad 0 \quad 0 \quad 0 \quad 0 \quad 0 \quad 0 \right] \phi_9(x)$$

$$\int_0^x \int_0^x \phi_{1,1}(x) dx dx = \left[\frac{-1}{6} \quad \frac{-1}{16} \quad 0 \quad \frac{1}{96} \quad 0 \quad 0 \quad 0 \quad 0 \quad 0 \right] \phi_9(x)$$

$$\int_0^x \int_0^x \phi_{1,2}(x) dx dx = \left[\frac{-1}{16} \quad \frac{-1}{12} \quad 0 \quad 0 \quad \frac{1}{192} \quad 0 \quad 0 \quad 0 \quad 0 \right] \phi_9(x)$$

$$\int_0^x \int_0^x \phi_{1,3}(x) dx dx = \left[\frac{3}{5} \quad \frac{5}{16} \quad 0 \quad 0 \quad 0 \quad \frac{1}{320} \quad 0 \quad 0 \quad 0 \right] \phi_9(x)$$

$$\int_0^x \int_0^x \phi_{1,4}(x) dx dx = \left[\frac{-7}{12} \quad \frac{-1}{10} \quad 0 \quad 0 \quad 0 \quad 0 \quad \frac{1}{480} \quad 0 \quad 0 \right] \phi_9(x)$$

Analysis of the operational matrix method studied in detail, [3], [21].

2.1.2 Method of Solution

Let us assume that

$$f^{iv}(\eta) = A^T \phi(\eta) \quad (3)$$

integrate Eq. (3) concerning η from 0 to η , we get,

$$f'''(\eta) = f'''(0) + A^T [P\phi(\eta) + \bar{\phi}(\eta)]. \quad (4)$$

Integrate (4) concerning from 0 to η

$$f''(\eta) = \eta f'''(0) + A^T [P'\phi(\eta) + \bar{\phi}'(\eta)] \quad (5)$$

Integrate (5) concerning η from 0 to η

$$f'(\eta) = f'(0) + \frac{\eta^2}{2} f'''(0) + A^T [P''\phi(\eta) + \bar{\phi}''(\eta)] \quad (6)$$

Integrate (6) concerning η from 0 to η

$$f(\eta) = \eta f'(0) + \frac{\eta^3}{6} f'''(0) + A^T [P'''\phi(\eta) + \bar{\phi}'''(\eta)] \quad (7)$$

Put $\eta = 1$ in (6) and (7) we get

$$\begin{aligned} f'''(0) &= 3 \left[A^T (P'''\phi(1) + \bar{\phi}'''(1)) \right] \\ f'(0) &= -A^T [P''\phi(1) + \bar{\phi}''(1)] - \frac{3}{2} [A^T (P''\phi(1) + \bar{\phi}''(1)) - 1 - A^T (P''\phi(1) + \bar{\phi}''(1))] \end{aligned} \quad (8)$$

Substitute these in (4) to (7)

$$f'''(\eta) = 3 \left[A^T (P'''\phi(1) + \bar{\phi}'''(1)) - 1 - A^T (P''\phi(1) + \bar{\phi}''(1)) \right] + A^T [P\phi(\eta) + \bar{\phi}(\eta)] \quad (9)$$

$$f''(\eta) = 3\eta \left[A^T (P''\phi(1) + \bar{\phi}''(1)) - 1 - A^T (P''\phi(1) + \bar{\phi}''(1)) \right] + A^T [P'\phi(\eta) + \bar{\phi}'(\eta)] \quad (10)$$

$$\begin{aligned} f'(\eta) &= -A^T [P''\phi(1) + \bar{\phi}''(1)] - \frac{3}{2} [A^T (P''\phi(1) + \bar{\phi}''(1)) - 1 - A^T (P''\phi(1) + \bar{\phi}''(1))] \\ &\quad + \frac{3\eta^2}{2} [A^T (P''\phi(1) + \bar{\phi}''(1)) - 1 - A^T (P''\phi(1) + \bar{\phi}''(1))] + A^T [P''\phi(\eta) + \bar{\phi}''(\eta)] \end{aligned} \quad (11)$$

$$\begin{aligned} f(\eta) &= \eta \left[-A^T (P''\phi(1) + \bar{\phi}''(1)) - \frac{3}{2} (A^T (P''\phi(1) + \bar{\phi}''(1)) - 1 - A^T (P''\phi(1) + \bar{\phi}''(1))) \right] \\ &\quad + \frac{\eta^3}{2} [A^T (P''\phi(1) + \bar{\phi}''(1)) - 1 - A^T (P''\phi(1) + \bar{\phi}''(1))] + A^T [P''\phi(\eta) + \bar{\phi}''(\eta)] \end{aligned} \quad (12)$$

Fit (3), (10), (11), (12), and (13) in (3) and collocate the resultant equation by subsequent collocation

points $\eta_i = \frac{2i-1}{2M}$ $i = 1, 2, \dots, M$. Then, solve this

system with the Newton-Raphson method, which yields unknown coefficients. Substitute these coefficients in (4.10), which gives the Hermite wavelet numerical solution.

3 Results and Discussions

The Hermite wavelet method is functional to solve the nonlinear differential equations arising in non-Newtonian heat transfer problems, and the disadvantages and advantages of this method are

discussed, [16]. Acceptable comparison is made with the earlier published work and validates the correctness of the numerical results, as shown in Table 1 (Appendix) and Table 2 (Appendix). The effects of the Casson fluid parameter γ , squeeze number S , and the magnetic variety at radial ($F'(\eta)$) and axial ($F(\eta)$) velocities are characterized.

a) Plates moving apart ($S > 0$)

In appendix section the Figure 1, Figure 2, Figure 3, Figure 4, Figure 5, Figure 6, Figure 7, Figure 8, describe how the squeeze number S behaves when the plates move apart. Figure 1 (Appendix) shows the properties of increasing values of S on the axial speed $F(\eta)$. It is evident increasing S effects in a decreased axial velocity. The property of increasing S on radial pace is shown in Figure 2 (Appendix). For rising S , an increase $F'(\eta)$ is pragmatic $0.5 < \eta \leq 1$; nevertheless, there is a decrease in $F'(\eta)$ is for $0 \leq \eta \leq 0.5$. Figure 3 (Appendix) depicts the behavior of γ on $F(\eta)$. An increase in γ slows down the axial flow. The effects of developing the Casson fluid parameter on radial velocity are proven in Figure 4 (Appendix). Increasing the Casson fluid parameter decreases $F'(\eta)$ for $0 \leq \eta \leq 0.5$ and an upward thrust in $F'(\eta)$ is determined for $0.5 < \eta \leq 1$.

In Figure 5, Figure 6, Figure 7, Figure 8 (Appendix), the effects of M_1 on $F(\eta)$ and $F'(\eta)$ are explained. It may be determined from Figure 5 (Appendix) and Figure 6 (Appendix) that for increasing magnetic number M_1 , and there may be a decrease in $F(\eta)$ for somewhat lower values of squeeze quantity S ; while for $F'(\eta)$, the growth in M_1 offers a velocity sketch comparable to the case of increasing S . Figure 7 and Figure 8 (Appendix) are pinched to investigate the results of magnetic area for barely better values of squeeze wide variety S . The conduct of radial and axial velocities remainder nearly much lower S .

b) Collapsing movement of the plates ($S < 0$)

In appendix section the Figure 9, Figure 10, Figure 11, Figure 12, Figure 13, Figure 14, Figure 15, Figure 16 are for the case when collapsing movement of the plates. In Figure 9 (Appendix), tremendous axial acceleration is found for declining S . Figure 10 (Appendix), represents the results of

decreasing S on radial velocity. It is understandable that $F'(\eta)$ increases with the squeeze charge for $0 \leq \eta \leq 0.4$. A surprising exchange in $F'(\eta)$ is found while $0.4 < \eta \leq 1$. Figure 11 and Figure 12 (Appendix) show the impacts of γ on radial and axial velocities, respectively. The same conduct is determined for γ and S when plates are approaching together.

Figure 13, Figure 14, Figure 15, Figure 16 (Appendix) gift properties' of the float while plates are approaching collectively ($S < 0$) and the M_1 is changing. In Figure 13 (Appendix), the results of increasing M_1 on $F(\eta)$ are shown, and a lower in $F(\eta)$ is discovered for larger values to some extent S . Figure 14 (Appendix) gives us a diagrammatical exhibition of $F'(\eta)$ for increasing M_1 . It represents $F'(\eta)$ decreases for $0 \leq \eta \leq 0.4$ however for $0.4 < \eta \leq 1$ it behaves in any other case, i.e., for increasing values of magnetic quantity, there's a speedy growth in radial speed of the liquid. A comparable behavior is determined for growing magnetic wide variety while $S = -10$ has more well-known consequences. Likewise, in Figure 16 (Appendix), a pretty speedy modification can be located for increasing values of the magnetic quantity. Also, the backflow can come out with a lower squeeze variety, and a physically powerful magnetic field is needed to decorate the stream, as proven in Figure 16 (Appendix).

4 Conclusion

An electrically conducting non-Newtonian fluid flow between two parallel plates is studied using the Hermite wavelet method. The basic equations are condensed using a similarity model to a single regular, highly nonlinear ordinary differential equation. Considering two cases, i.e., One while plates are transferring apart and the other when plates are approaching nearer. HWM is applied to resolve the basic equation that goes with the flow. The properties of up-and-coming known parameters on glide are verified graphically, and a complete dialogue is provided. A numerical answer is also acquired using the RK-four method, VPM, to evaluate the effects received by HWM, and some of the answers determine remarkable conformity. It can be seen from the figures that a robust magnetic field may be second-hand to decorate the float while plates are approaching jointly, and squeeze variety

increases the velocity sketch for both cases, i.e., while plates are approaching nearer and while plates are leaving aside. Further, Squeeze flow is studied by considering different types of non-Newtonian fluids.

References:

- [1] V. Mishra, Haar Wavelet Approach to Fluid Flow between Parallel Plates, *International Journal of Fluids Engineering*, Vol. 3, No. 4, 2011, pp. 403-410.
- [2] H. Karkera, N. N. Katagi, and R. B. Kudenatti, Analysis of general unified MHD boundary-layer flow of a viscous fluid - a novel numerical approach through wavelets, *Mathematics and Computers in Simulation*, Vol. 168, 2020, pp. 135-154.
- [3] S. Kumbinarasaiah and K. R. Raghunatha, Numerical solution of the Jeffery–Hamel flow through the wavelet technique, *Heat Transfer*, Vol. 51, No. 2, 2022, pp. 1568-1584.
- [4] M. Khaksar-e Oshagh, M. Abbaszadeh, E. Babolian, and H. Pourbashash, An adaptive wavelet collocation method for the optimal heat source problem, *International Journal of Numerical Methods for Heat & Fluid Flow*, Vol. 32, No. 7, 2022, pp. 2360-2382.
- [5] M. Usman, T. Zubair, M. Hamid, R. U. Haq, and Z. H. Khan, Unsteady flow and heat transfer of tangent-hyperbolic fluid: Legendre wavelet-based analysis, *Heat Transfer*, Vol. 50, 2021, pp. 3079– 3093.
- [6] N. Ahmed, U. Khan, S. I. Khan, S. Bano, and S. T. Mohyud-Din, Effects on magnetic field in squeezing flow of a Casson fluid between parallel plates, *Journal of King Saud University-Science*, Vol. 29, No. 1, 2017, pp. 119-125.
- [7] M. J. Stefan, Experiment on apparent adhesion, proceedings of the Academy of Sciences in Vienna Mathematics-Natural Knowledge (Versuch Uber die scheinbare adhesion, Sitzungsberichteder Akademie der Wissenschaften in Wien Mathematik-Naturwissen), Vol. 69, 1874, pp. 713–721.
- [8] O. Reynolds, IV. On the theory of lubrication and its application to Mr. Beauchamp tower's experiments, including an experimental determination of the viscosity of olive oil, *Philosophical Transactions of the Royal Society of London*, Vol. 177, 1889, pp. 157-234.

[9] F. R. Archibald, Load capacity and time relations for squeeze films, *Transactions of the ASME*, Vol. 78, No. 1, 1956, pp. 29-35.

[10] R. Usha and R. Sridharan, "Arbitrary squeezing of a viscous fluid between elliptic plates," *Fluid Dynamics Research*, Vol. 18, No. 1, 1996, pp. 35-51.

[11] G. Birkhoff, *Hydrodynamics*, Princeton University Press, Vol. 2234, 2015.

[12] C. Y. Wang and L. T. Watson, Squeezing of a viscous fluid between elliptic plates, *Applied Scientific Research*, Vol. 35, No. 2, 1979, pp. 195-207.

[13] A. M. Siddiqui, S. Irum, and A. R. Ansari, Unsteady squeezing flow of a viscous MHD fluid between parallel plates, a solution using the homotopy perturbation method, *Mathematical Modelling and Analysis*, Vol. 13, No. 4, 2008, pp. 565-576.

[14] M. Mustafa, T. Hayat, and S. Obaidat, On heat and mass transfer in the unsteady squeezing flow between parallel plates, *Meccanica*, Vol. 47, 2012, pp. 1581-1589.

[15] C. Vlachopoulos, M. O'Rourke, and W. W. Nichols, *McDonald's Blood Flow in Arteries: Theoretical, Experimental and Clinical Principles*, 6th ed. CRC Press, 2011. DOI: 10.1201/b13568.

[16] [16] V. G. Nikitaev, V. O. Nagornov, A. N. Pronichev, E. V. Polyakov, and V. V. Dmitrieva, The use of the wavelet transform for the formation of the quantitative characteristics of the blood cells images for the automation of hematological diagnostics, *WSEAS transactions on biology and biomedicine*, Vol.12(3), 2015, pp.16-19.

[17] Y. K. Demyanovich, Parallelization of Spline-Wavelet Decomposition, *WSEAS Transactions on Mathematics*, Vol.18, 2019, pp.241-249.

[18] S. Postalcioglu, Wavelet transform based feature extraction for EEG signal classification, *WSEAS Transactions on Computers*, Vol. 20, 2021, pp.199-206, <https://doi.org/10.37394/23205.2021.20.21>.

[19] Y. K. Dem'yanovich, O. N. Ivantsova, and A. Y. Ponomareva, Continuum Wavelets and Distributions, *WSEAS Transactions on Mathematics*, Vol. 21, 2022, pp.553-562, <https://doi.org/10.37394/23206.2022.21.62>.

[20] Y. U. R. I. Dem'yanovich, and B. I. C. H. Le Thi Nhu, Discrete and Continuous Wavelet Expansions, *WSEAS Transactions on Mathematics*, Vol. 21, 2022, pp.58-67, <https://doi.org/10.37394/23206.2022.21.9>.

[21] S. Kumbinarasaiah, K. R. Raghunatha, M. Rezazadeh, and M. Inc, A solution of coupled nonlinear differential equations arising in a rotating micropolar nanofluid flow system by Hermite wavelet technique, *Engineering with Computers*, Vol. 38, 2022, pp. 3351-3372.

APPENDIX

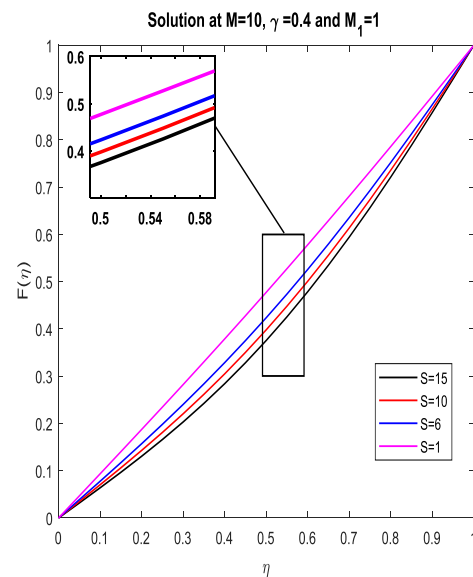


Fig. 1: Variation of $F(\eta)$ for different values of S .

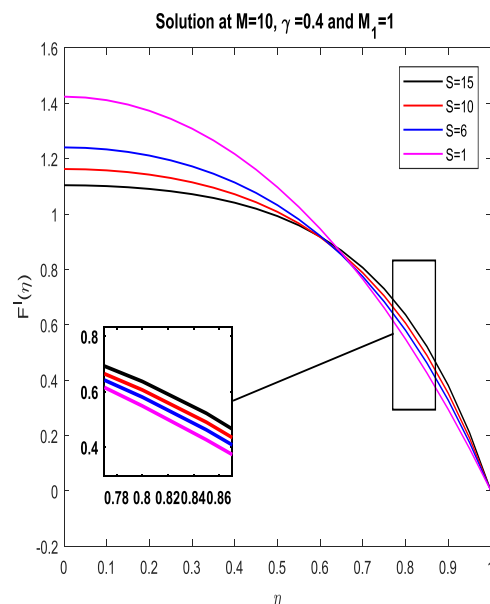


Fig. 2: Variation of $F'(\eta)$ for different values of S .

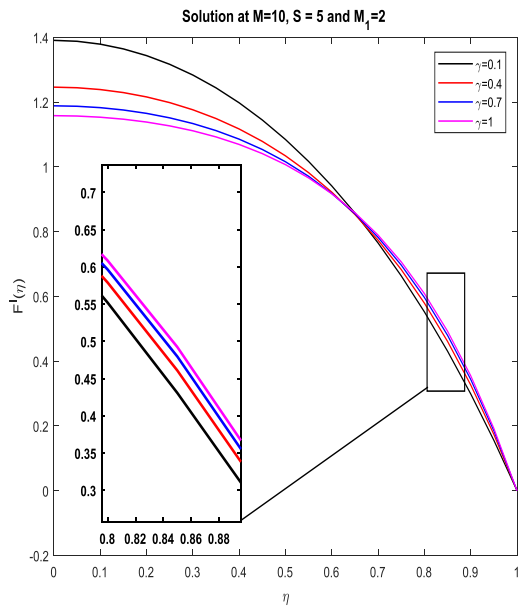


Fig. 3: Variation of $F'(\eta)$ for different values of γ .

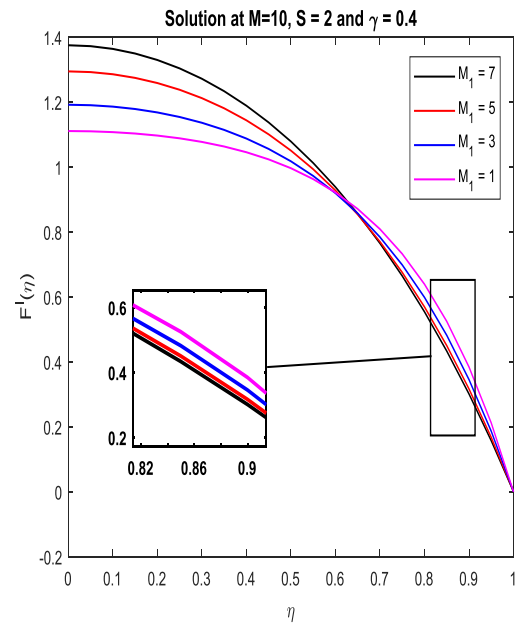


Fig. 5: Variation of $F'(\eta)$ for different values of M_1 .

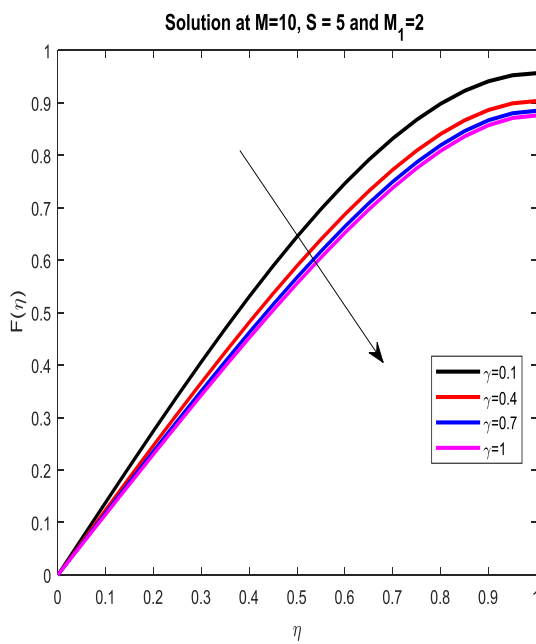


Fig. 4: Variation of $F(\eta)$ for different values of γ .

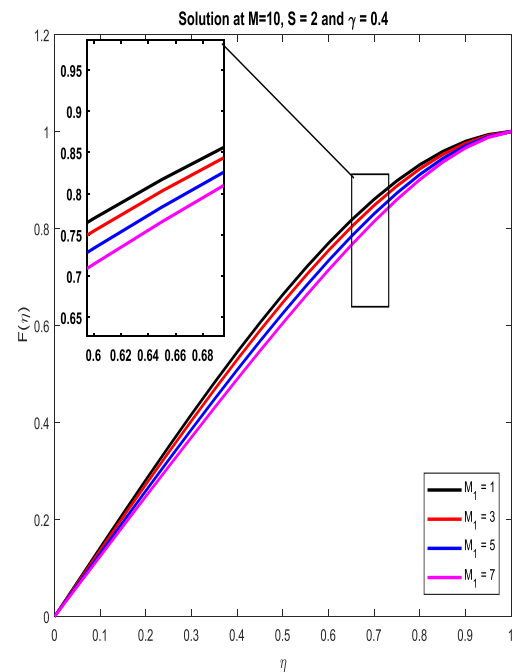


Fig. 6: Variation of $F(\eta)$ for different values of M_1 .

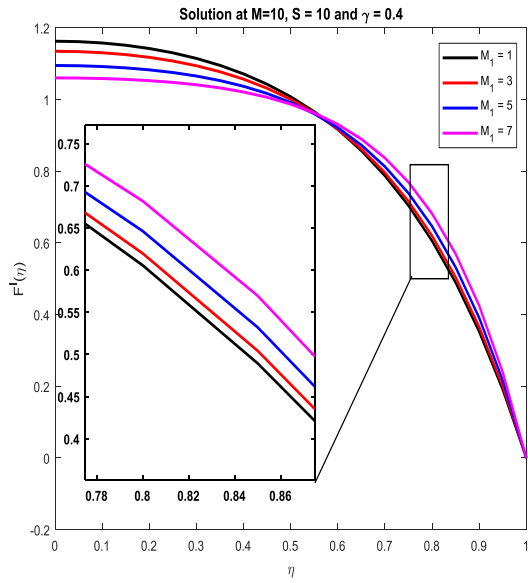


Fig. 7: Variation of $F'(\eta)$ for different values of M_1 .

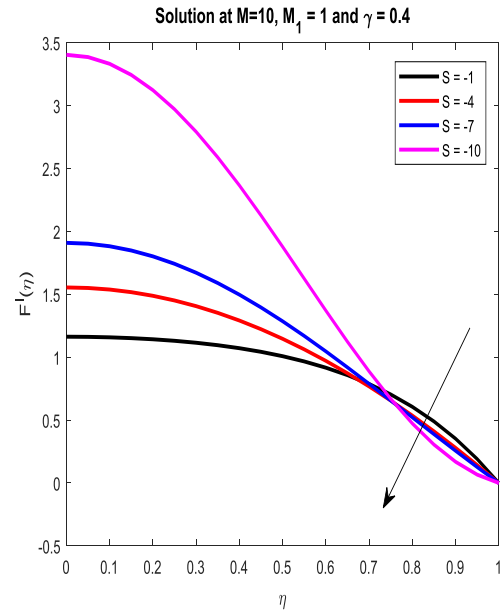


Fig. 9: Variation of $F'(\eta)$ for different negative values of S .

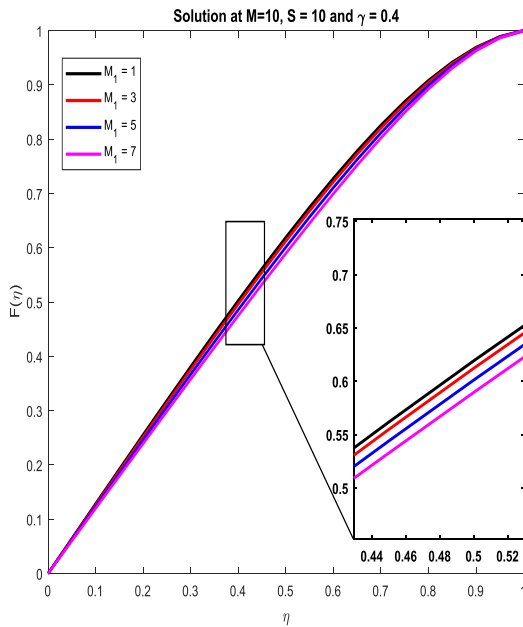


Fig. 8: Variation of $F(\eta)$ for different values of M_1 .

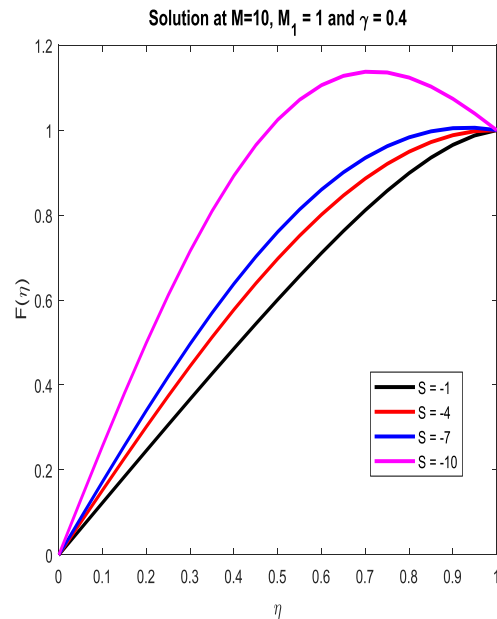


Fig. 10: Variation of $F(\eta)$ for different negative values of S .

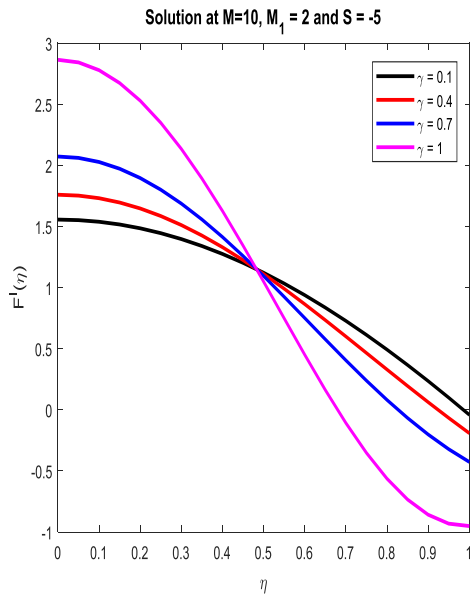


Fig. 11: Variation of $F'(\eta)$ for different values of γ .

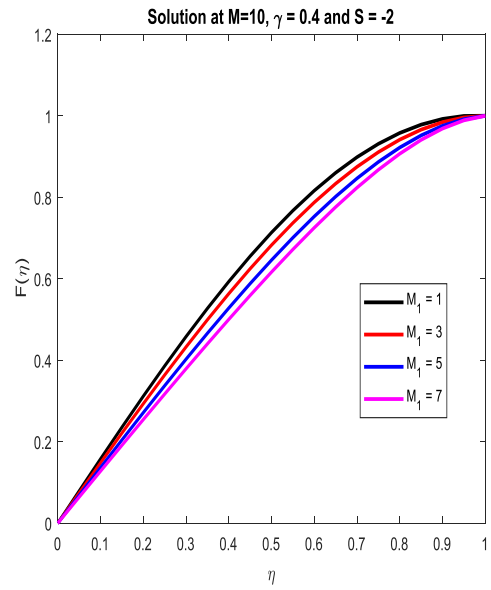


Fig. 13: Variation of $F(\eta)$ for different values of M_1 .

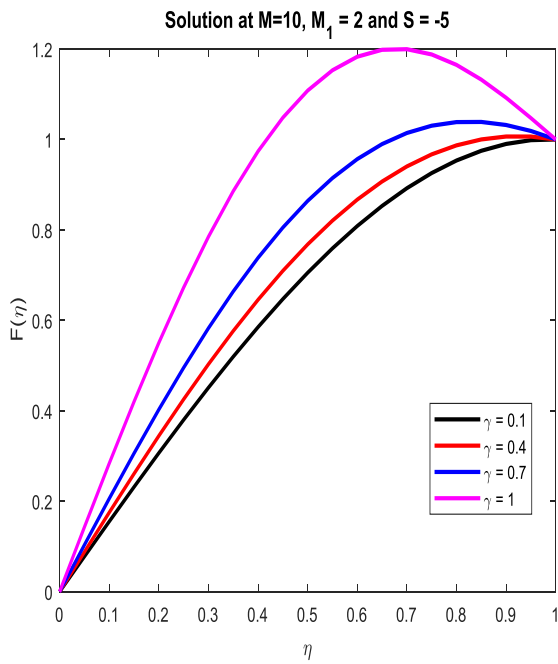


Fig. 12: Variation of $F(\eta)$ for different values of γ .

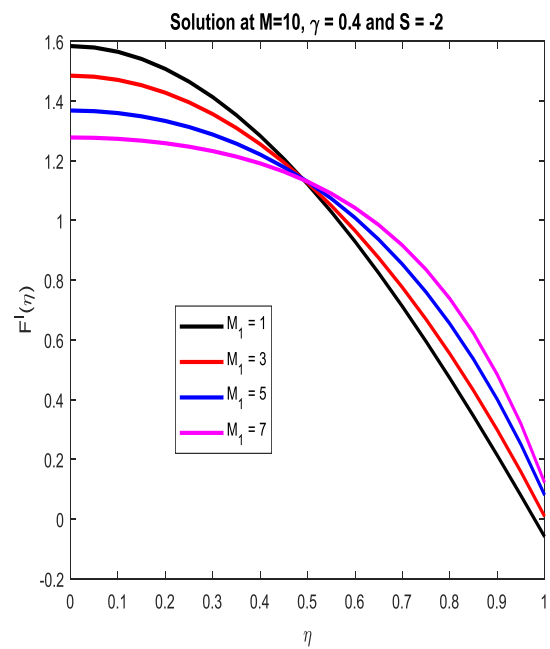


Fig. 14: Variation of $F'(\eta)$ for different values of M_1 .

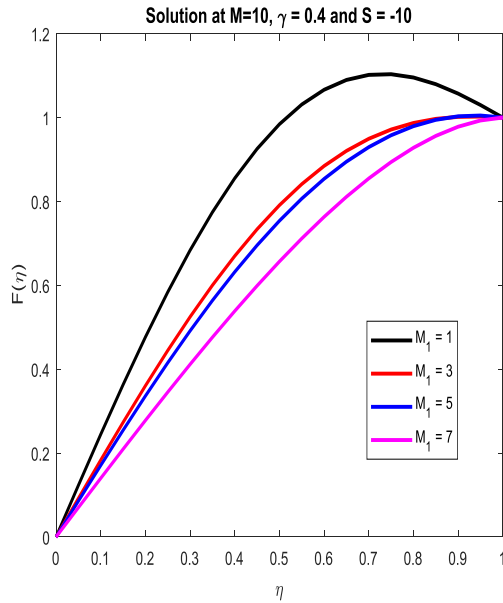


Fig. 15: Variation of $F(\eta)$ for different values of M_1 .

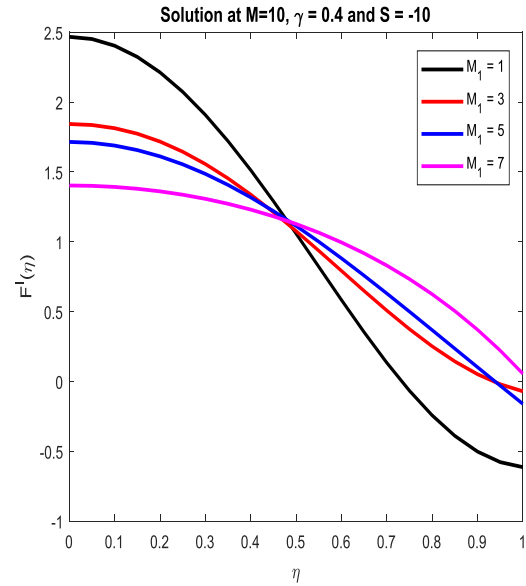


Fig. 16: Variation of $F'(\eta)$ for different values of M_1 .

Table 1. Comparison between the VPM, HWM, and numerical results for $\gamma = 0.4$ and $M_1 = 1$.

η	$S = 5$						$S = -5$					
	$F(\eta)$			$F'(\eta)$			$F(\eta)$			$F'(\eta)$		
	VPM	HWM	Numerical	VPM	HWM	Numerical	VPM	HWM	Numerical	VPM	HWM	Numerical
0	0	0	0	1.359393	1.359393	1.359393	0	0	0	1.677216	1.677216	1.677216
0.1	0.139081	0.139081	0.139081	1.348452	1.348452	1.348452	0.166839	0.166839	0.166839	1.650804	1.650804	1.650804
0.2	0.276358	0.276358	0.276358	1.357517	1.357517	1.357517	0.328444	0.328444	0.328444	1.572994	1.572994	1.572994
0.3	0.409918	0.409918	0.409918	1.310148	1.310148	1.310148	0.479861	0.479861	0.479861	1.447971	1.447971	1.447971
0.4	0.537628	0.537628	0.537628	1.239953	1.239953	1.239953	0.616685	0.616685	0.616685	1.282424	1.282424	1.282424
0.5	0.657014	0.657014	0.657014	1.142869	1.142869	1.142869	0.735286	0.735286	0.735286	1.085120	1.085120	1.085120
0.6	0.765125	0.765125	0.765125	1.013414	1.013414	1.013414	0.832992	0.832992	0.832992	0.866366	0.866366	0.866366
0.7	0.858383	0.858383	0.858383	0.844480	0.844480	0.844480	0.908218	0.908218	0.908218	0.637365	0.637365	0.637365
0.8	0.932408	0.932408	0.932408	0.627096	0.627096	0.627096	0.960506	0.960506	0.960506	0.409532	0.409532	0.409532
0.9	0.981819	0.981819	0.981819	0.350136	0.350136	0.350136	0.990529	0.990529	0.990529	0.193804	0.193804	0.193804
1.0	1	1	1	0	0	0	1	1	1	0	0	0

Table 2. Numerical values and HWM for skin friction coefficient.

S	γ	M	$\left(1 + \frac{1}{\gamma}\right) F''(1)$	$\left(1 + \frac{1}{\gamma}\right) F''(1)$
			[6]	HWM
-5.0			-6.298708	-6.298700
-3.0			-8.320727	-8.320731
-1.0			-9.970376	-9.970303
1.0			-11.376240	-11.376224
3.0			-12.610669	-12.610675
5.0			-13.718095	-13.718073
-3.0	0.1		-30.991005	-30.991088
	0.3		-10.873387	-10.873323
	0.5		-6.771549	-6.771515
3.0	0.1		-35.260196	-35.260155
	0.3		-15.149577	-15.149564
	0.5		-11.078736	-11.078727
-3.0	0.4	2	-13.101572	-13.101587
		4	-14.908219	-14.908243
		6	-17.501183	-17.501128
3.0	0.4	2	-9.038196	-9.0381932
		4	-11.531983	-11.531954
		6	-14.819321	-14.819334

Contribution of Individual Authors to the Creation of a Scientific Article (Ghostwriting Policy)

The authors equally contributed to the present research, at all stages from the formulation of the problem to the final findings and solution.

Sources of Funding for Research Presented in a Scientific Article or Scientific Article Itself

No funding was received for conducting this study.

Conflict of Interest

The authors have no conflicts of interest to declare.

Creative Commons Attribution License 4.0 (Attribution 4.0 International, CC BY 4.0)

This article is published under the terms of the Creative Commons Attribution License 4.0

https://creativecommons.org/licenses/by/4.0/deed.en_US